

RESEARCH

Open Access



Synthesis, crystal structural description, DNA binding, molecular docking, and anticancer evaluation of the novel platinum(IV) supramolecular complex

Doaa Domyati^{1*}, Ehab M. M. Ali^{2,3}, Mostafa A. Hussien^{4,5}, Bambar Davaasuren⁶, Mariusz Jaremko⁷ and Mohamed M. El-bendary^{1,8*}

Abstract

A novel platinum(IV) supramolecular complex; $[\text{PtCl}_2(2,2'\text{-bipy})_2](\text{PtCl}_6)$ was synthesized in aqueous acetonitrile solution at ambient temperature with constant stirring. The structure was confirmed by elemental analysis, FT-IR, UV-vis, NMR spectroscopy, and single-crystal X-ray diffraction, revealing a unique distorted octahedral geometry and a three-dimensional network stabilized by hydrogen bonding and π - π stacking. DNA binding studies, including electronic absorption titration and viscometry, indicated a groove binding mechanism with a binding constant (K_b) of $5.00 \times 10^6 \text{ M}^{-1}$. Molecular docking with DNA (PDB ID: 1BNA) and cancer-related proteins (PDB codes: 3ig7, 3eqm, 4fm9) supports these interactions, while in vitro anticancer assays demonstrated potent cytotoxicity with IC_{50} values of $41.37 \mu\text{M}$ for HepG2, $47.62 \mu\text{M}$ for HCT116, and $73.90 \mu\text{M}$ for MDA-MB-231 cells, outperforming cisplatin in selectivity. This study not only advances our understanding of structure-activity relationships in platinum-based complexes but also highlights the potential of this complex as a promising candidate for developing more effective and less toxic anticancer agents.

Keywords Anticancer evaluation, DNA binding, Molecular docking, Platinum(IV), Structural characterization, 2,2'-Bipyridine

*Correspondence:

Doaa Domyati
Dmdomyati@uj.edu.sa
Mohamed M. El-bendary
mmesmaeel@uj.edu.sa

¹ College of Science, Department of Chemistry, University of Jeddah, 21959 Jeddah, Saudi Arabia

² Biochemistry Department, Faculty of Science, King Abdulaziz University, 21589 Jeddah, Saudi Arabia

³ Division of Biochemistry, Department of Chemistry, Faculty of Science, Tanta University, Tanta 31527, Egypt

⁴ Department of Chemistry, Faculty of Science, King Abdulaziz University, P.O. Box 80203, 21589 Jeddah, Saudi Arabia

⁵ Department of Chemistry, Faculty of Science, Port Said University, Port Said 42521, Egypt

⁶ Core Labs, King Abdullah University of Science and Technology (KAUST), 23955-6900 Thuwal, Saudi Arabia

⁷ Biological and Environmental Science and Engineering (BESE) Division, King Abdullah University of Science and Technology (KAUST), 23955-6900 Thuwal, Saudi Arabia

⁸ Chemistry Department, Faculty of Science, Tanta University, Tanta 31527, Egypt



© The Author(s) 2025. **Open Access** This article is licensed under a Creative Commons Attribution-NonCommercial-NoDerivatives 4.0 International License, which permits any non-commercial use, sharing, distribution and reproduction in any medium or format, as long as you give appropriate credit to the original author(s) and the source, provide a link to the Creative Commons licence, and indicate if you modified the licensed material. You do not have permission under this licence to share adapted material derived from this article or parts of it. The images or other third party material in this article are included in the article's Creative Commons licence, unless indicated otherwise in a credit line to the material. If material is not included in the article's Creative Commons licence and your intended use is not permitted by statutory regulation or exceeds the permitted use, you will need to obtain permission directly from the copyright holder. To view a copy of this licence, visit <http://creativecommons.org/licenses/by-nc-nd/4.0/>.

Introduction

Cancer is a major health problem worldwide [1]. Chemotherapy is one of the primary cancer treatment modalities [2, 3]. One drug being researched to treat cancer is clinically approved cisplatin, which has shown promise in treating several cancer types [4]. However, cisplatin has drawbacks, including severe side effects, lack of selectivity towards cancer cells, and developed resistance to cancer cells. Therefore, one of the main objectives of scientific study is the design of new materials, such as supramolecular complexes with distinctive structures that can be used as safe anticancer medications [5, 6]. Among the most significant features of supramolecular platinum complexes are their structural diversity and possible biological and anticancer activities applications [7–12]. Therefore, there is a need to design and develop good drugs of platinum complexes, which can be done through pre-clinical testing and provide information on the drug's mechanism of action. Cancer remains a global health challenge, and platinum-based drugs such as cisplatin, while effective, often suffer from severe side effects and resistance issues.

Following cisplatin's approval for use in humans, other platinum complexes have been developed and examined to address some of the drawbacks of the medication, including inherent or acquired resistance and serious side effects primarily resulting from cisplatin's lack of selectivity. As a result, in contrast to cisplatin, novel platinum complexes with increased therapeutic efficacy are being developed globally [12]. Platinum compounds, like cisplatin, have been well-established for their potent anticancer activities, yet there is an ongoing need to discover new platinum complexes that offer improved therapeutic efficacy with fewer side effects [13]. New platinum medicines with lower toxicity can be created by attaching the platinum coordination moiety to a suitable carrier ligand that targets cancer cells preferentially [14]. Investigating and creating multi-action Pt(IV) complexes with possible anticancer properties is a recent trend in this field [15, 16]. The square planar Pt(II) complexes with two additional ligands positioned in the axial locations can be considered octahedral Pt(IV) complexes. Although octahedral low-spin d⁶-metal is relatively inert to ligand substitution, Pt(IV) is a good prodrug that can be triggered inside cancer cells. But the reduction can be made stronger to produce the original Pt(II) medication along with the two free axial ligands [17]. DNA and BSA (Bovine Serum Albumin) are strongly bound by Pd(II) and Pt(IV) supramolecular complexes that include nitrogen pyridine bases [18]. By inducing apoptosis, intracellular ROS generation, and S-phase cell cycle arrest, some of these complexes significantly

suppress the proliferation of MCF-7, T47D breast cancer cells, and HCT116 colon cancer cells [18]. The effectiveness of platinum complexes in oncology is largely due to their ability to bind to DNA, thereby interfering with cell replication and triggering apoptosis. Understanding, the molecular docking and DNA binding mechanisms of Pt complexes is crucial for developing new and more effective drugs with fewer side effects.

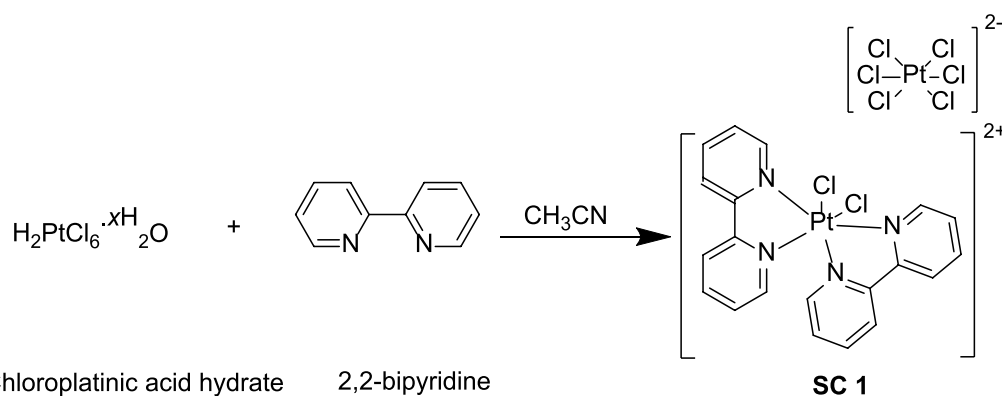
Molecular docking and DNA binding studies play essential roles in evaluating the anticancer potential of these novel complexes [19]. Molecular docking allows for the prediction and visualization of how these complexes interact with specific biological targets, such as proteins or DNA. DNA binding studies are equally important, as they help to determine how the platinum complex interacts with DNA, a critical target for many anticancer drugs [20]. The efficacy of a platinum complex is often linked to its ability to bind to DNA, leading to DNA damage, interference with replication processes, and triggering of apoptosis in cancer cells [21]. By examining the DNA binding affinity and mode of interaction (such as intercalation, groove binding, or covalent attachment), these studies enhance our understanding of the complex's mechanism of action and its potential as an anticancer agent [20–22].

Therefore, a novel Pt(IV) supramolecular complex with 2,2'-bipyridine (2,2'-bipy) ligand [PtCl₂(2,2'-bipy)₂] (PtCl₆), (**SC 1**) was created and given a structural characterization to look into how it affected the growth of various cancer cell lines; HepG2, HCT116, MDA. Furthermore, the cytotoxicity of the synthesized **SC 1** will be examined towards a normal cell line. DNA binding and molecular docking were examined.

Experimental

Materials and instrumentation

The analytical grade chemicals, (2,2'-Bipyridine 99% and Chloroplatinic acid 98%) solvents, and reagents utilized in the synthesis were all acquired from Sigma-Aldrich and used exactly as supplied, requiring no additional cleaning. A PerkinElmer Spectrum 100 instrument was used to obtain the infrared (IR) spectra of **SC 1**, which was formulated as a KBr disk. The reported bands are in cm⁻¹. The Bruker Avance 800 MHz spectrometer was used to obtain the ¹H (800 MHz) and ¹³C (151 MHz) NMR spectra, which were referenced to residual DMSO signals {DMSO-*d*₆: ¹H (2.50)/¹³C (39.5)}. An automatic elemental analyzer, the Perkin-Elmer 2400, was used to conduct elemental analyses (C, H, and N). An electronic spectrometer (Shimadzu UV-310 I PC) recorded the absorption spectra. A Cary Eclipse Fluorescence Spectrophotometer was used to measure the fluorescent spectra.



Scheme 1 Synthetic pathway of **SC 1**

Synthesis of $[\text{PtCl}_2(2,2'\text{-bipy})_2](\text{PtCl}_6)$, (**SC 1**)

In aqueous acetonitrile (30 mL) at ambient temperature, a solution of chloroplatinic acid hydrate; $\text{H}_2\text{PtCl}_6 \cdot x\text{H}_2\text{O}$ (0.102 g, 0.25 mmol) was mixed with 2,2'-Bipyridine (2,2'-bipy) (0.078 g, 0.5 mmol), Scheme 1. After stirring for 30 min, the mixture was sealed and allowed to evaporate gradually. Yellow prismatic crystals appeared after 10 days, which were washed with acetonitrile and air-dried. The yield was 135 mg (60% mass yield). Analytical data for the molecular formula $\text{C}_{20}\text{H}_{16}\text{N}_4\text{Cl}_8\text{Pt}_2$, **1**: Calcd. C, 24.36; H, 1.64; N, 5.68; Found: C, 24.55%; H, 1.59; N, 5.87. IR, KBr (cm^{-1}) (s, strong; m, medium; w, weak): 3056 w, 1617 m, 1590 m, 1542 s, 1507 s, 1415 s, 1340 w, 1219 s, 1139 m, 1092 m, 843 vs, 768 m, 710 vs.

Determination of a single crystal structure

Single-crystal X-ray diffraction experiments were used to produce and describe the structure of single crystals of $\text{C}_{20}\text{H}_{16}\text{N}_4\text{Cl}_8\text{Pt}_2$, **SC1**. The single crystal data collection was carried out on *IuS 2* microsource Bruker D8 Venture diffractometer using $\text{Mo K}\alpha$ ($\lambda = 0.71073$ Å) radiation at 120.00 K. After employing Olex2 [23], the structure was solved using the Intrinsic Phasing method in the SHELXT [24] structure solution tool, and the Least Squares minimization method in the SHELXL [25] refinement package. Many crystals from different batches were screened and the best quality crystal was used for the full data collection. The quality of the crystal was not very good as the final refinement still shows largest difference peak/hole pair of 1.58/1.18 $\text{e} \text{ \AA}^{-3}$, near the Pt atoms. We assume that this could be related to the quality of the crystal, absorption correction due to heavy Pt atom. Inspection of the reflection file did not suggest presence of any twinning. However,

the presence of a small fraction of intergrown domain could not be rule out.

Studies of DNA binding

DNA binding studies were conducted using electronic absorption titration and viscometric techniques. The results indicate groove binding with a binding constant (K_b) of $5.00 \times 10^6 \text{ M}^{-1}$.

Determination of binding affinities spectroscopically

To assess the binding affinity of the **SC 1** with CT-DNA, absorption spectra were measured with DNA's intrinsic absorption subtracted. Solutions were prepared using 5 mM Tris-HCl buffer (pH 7.40) and 50 mM NaCl, preserving a constant concentration of 20 μM for **SC1**. Since **SC1** has poor solubility in aqueous solutions, 5% DMSO was added to improve solubility. The ratio of $[\text{DNA}]/[\text{SC 1}]$ was varied from 0 to 8.0. The (K_b) was calculated using the equation from the titration process:

$$\begin{aligned} & ([\text{DNA}]) / ((\epsilon_A - \epsilon_F)) \\ &= ([\text{DNA}]) / ((\epsilon_B - \epsilon_F)) \\ &+ 1/K_b (\epsilon_B - \epsilon_F) \end{aligned}$$

as ϵ_A , ϵ_B and ϵ_F represent the extinction coefficients of the **SC 1** at a specific DNA addition, before DNA addition, and at the fully bound state. By plotting $[\text{DNA}]/(\epsilon_A - \epsilon_F)$ against $[\text{DNA}]$, K_b can be obtained [26].

Viscometry-based binding mode determination

Viscosity study conducted by an Ostwald viscometer. (10 μL) of platinum(IV) complex added to a ct-DNA solution, maintaining a $[\text{SC 1}]/[\text{DNA}]$ ratio between 0.02 and 0.2. The mixtures incubated for 5 min at 26 $^\circ\text{C}$ in a water bath. Flow times for the solutions verified

and repeated at least three times for accuracy. The relative viscosity $(\eta/\eta^0)^{1/3}$ was plotted against the [SC 1]/[DNA] ratio, where η is the specific viscosity of ct-DNA alone and η^0 is the specific viscosity of the ct-DNA-SC 1. Specific viscosities were calculated [27, 28].

Molecular docking study of SC 1 with DNA and three different cancer proteins

The study explored the molecular interactions of SC 1, a compound theoretically binding to DNA, with three distinct active proteins, analyzing their effects on cell proliferation, receptor functions, cell membrane reliability, and DNA conformation. Molecular docking techniques were employed using the DNA sequence 1BNA [29], cyclin-dependent kinase 5 (Cdk5) in colon cancer (PDB code: 3ig7) [29], aromatase cytochrome P450 in breast cancer (PDB code: 3eqm) [30], and topoisomerase in liver cancer (PDB code: 4fm9) [31]. All docking simulations were conducted on the MOE 2019.102 platform, modeling interactions in both 2D and 3D. The binding energies (E) and chemical interactions between SC 1 and the targets were analyzed.

The 3D structures of all proteins are reclaimed as PDB files from (<https://www.rcsb.org/>; accessed on June 3, 2024), were processed by removing solvent molecules and correcting structures and charges according to prior methods [32]. Active sites, distinct by the attendance of active drugs or co-crystallized ligands, and isolated as dummy atoms. The molecular docking was performed using Triangle Matcher with rigid protein, and scores were calculated with the top 5 poses selected. The results were assessed based on the docking score (S), the root-mean-square deviation (RMSD) between the co-crystallized and docked conformations.

Viability assessments of human cell lines treated with SC 1

King Abdulaziz University's Tissue Culture Unit in the Department of Biochemistry provided three human breast cell lines: HepG2, HCT116, and MDA. These cell lines were cultured in T75 flasks with complete media DMEM (bought from Gibco Life Technologies) for 24 h. The media contained 10% fetal bovine serum (FBS) and 1% antibiotic. After that, the flasks were kept in an incubator with 5% CO₂ at 37 °C and 95% humidity. To separate the adherent cells, 4 mL of 0.25% Trypsin was added to the T75 flask after the cells had grown to 90% confluency. The mixture was then incubated for 5 min at 37 °C. The pellets were suspended in complete media and counted by hemacytometer after staining by 0.4% trypan blue.

Each well of a 96-well microplate received 5000 cells in 0.1 mL of the complete media. The plate was then

incubated for a full day. The SC 1 was soluble in DMSO and stable under light and air. DMSO is used to stop the degradation of biological materials that are sensitive to temperature, such as organic compounds and serum. It can also be used on heat and light stabilizers to prevent changes in their physicochemical characteristics caused by heat and light. Each well containing attached cells received varying quantities of SC 1 (range from 6.25 to 100 µg/mL) dissolved in full DMEM medium. Every complex concentration resulted in the repetition of three wells and incubated in a CO₂ incubator for 48 h. After adding 100 µL of 0.5 mg MTT/mL free media to each well, the incubation was left in the dark for 3 h. Each well was filled with 100 µL of MTT medium, then filled with 100 µL of DMSO and incubated for 15 min. The wells were read using a Japanese Bio-RAD microplate reader that was calibrated to 595 nm. The complex's half maximum inhibitory concentrations (IC₅₀s), which prevented 50% of cells from developing, were determined using the software GraphPad Prism 9. This was ascertained using a curve that plotted the proportion of viable cells against the concentrations of SC 1. [33, 34].

The SC 1 and cisplatin were assessed for cytotoxicity against normal MRC5 cell lines in vitro. To determine the cytotoxic selectivity of cancer cells relative to normal cells (MRC5), the selectivity index was calculated using the following formula:

$$SI = IC_{50} \text{ normal cells} / IC_{50} \text{ cancer cells}$$

Results and discussion

Description of crystal structure of [PtCl₂(2,2'-bipy)₂](PtCl₆), SC 1

At room temperature (25 °C), 2,2'-bipy and chloroplatinic acid hydrate mixed to produce a supramolecular complex (SC 1). In DME, SC 1 dissolves readily and is stable in both air and light. In the monoclinic system, SC 1 crystallizes with space group C2/c. Table 1 shows the crystallographic characteristics parameters, while, Table 2 displays bond lengths and angles. One 2,2'-bipy ligand, one chloride ion, one platinum (IV) atom, and one half of a [Pt(Cl)₆]²⁻ anionic complex constitute the asymmetric unit of SC 1 (Fig. 1a). The half formula unit builds up the asymmetric unit of SC 1, since the Pt atoms serve as the center of inversion. Two repeating asymmetric units of the molecular structure of SC 1, which includes platinum (IV), two chloride ions, two 2,2'-bipy ligands, and [Pt(Cl)₆]²⁻ complex, are depicted in the ORTEP diagram in Fig. 1b. The supramolecular complex 1 is comprised of two ionic complexes; [Pt(Cl)₆]²⁻ an anionic complex, and [PtCl₂(2,2'-bipy)₂]²⁺, a cationic complex (Fig. 1b). The anionic complex of [Pt(Cl)₆]²⁻ consists of six chloride ions that coordinate Pt2 in an octahedral environment

Table 1 Crystallographic parameters and unit cell dimensions, space group, density, and refinement statistics for **SC 1**

Empirical formula	C ₂₀ H ₁₆ N ₄ Cl ₈ Pt ₂
CCDC number	2307870
Formula weight	986.15
Temperature/K	120.00
Crystal system	monoclinic
Space group	C2/c
a/Å	21.842 (9)
b/Å	7.398 (3)
c/Å	17.062 (6)
α/°	90
β/°	103.944 (12)
γ/°	90
Volume/Å ³	2675.6 (18)
Z	4
ρ _{calc} /g/cm ³	2.448
μ/mm ⁻¹	11.264
F(000)	1824.0
Crystal size/mm ³	0.225 × 0.127 × 0.112
Radiation	MoKα (λ = 0.71073)
2θ range for data collection/°	3.842 to 53.992
Index ranges	-27 ≤ h ≤ 27, -9 ≤ k ≤ 9, -21 ≤ l ≤ 21
Reflections collected	22,532
Independent reflections	2888 [R _{int} = 0.0759, R _{sigma} = 0.0474]
Data/restraints/parameters	2888/0/157
Goodness-of-fit on F ²	1.081
Final R indexes [I > 2σ (I)]	R ₁ = 0.0323, wR ₂ = 0.0710
Final R indexes [all data]	R ₁ = 0.0349, wR ₂ = 0.0733
Largest diff. peak/hole/e Å ⁻³	1.58/- 1.18

Table 2 Geometric parameters of selected bond lengths (Å) and bond angles (°) for **SC 1**

Bond	Å d	Bond	Deg, °
Pt1-Cl1 ^a	2.3025 (13)	Cl1-Pt1-Cl1 ^a	89.75 (7)
Pt1-Cl1	2.3024 (13)	N1-Pt1-Cl1 ^a	86.34 (11)
Pt1-N1 ^a	2.029 (4)	N1-Pt1-Cl1	96.66 (11)
Pt1-N1	2.029 (4)	N1 ^a -Pt1-Cl1	86.34 (11)
Pt1-N2	2.045 (4)	N1-Pt1-N1 ^a	175.79 (18)
Pt1-N2 ^a	2.045 (4)	N1-Pt1-N2 ^a	80.54 (16)
Pt2-Cl2	2.3378 (13)	N1-Pt1-N2	96.45 (14)
Pt2-Cl2 ^b	2.3378 (14)	Cl4-Pt2-Cl3	91.46 (4)
Pt2-Cl3 ^b	2.3269 (14)	Cl4-Pt2-Cl3 ^b	88.54 (5)
Pt2-Cl3	2.3269 (15)	Cl4 ^b -Pt2-Cl3 ^b	91.46 (5)
Pt2-Cl4 ^b	2.3268 (12)	Cl4-Pt2-Cl2	89.89 (6)
Pt2-Cl4	2.3267 (12)	Cl4-Pt2-Cl4 ^b	180.00

^a 1-X, +Y, 1/2-Z^b 1/2-X, 3/2-Y, 1-Z

that is slightly distorted. The Pt(IV) atom acts as the center of inversion, as shown in Fig. 1b. The cis ∠Cl–Pt–Cl lies in the range of 89.23(5)°–91.46(5)°, and the three crystallographically independent Pt–Cl bond lengths are almost similar within the range of 2.327(13)–2.329(13) Å, Table 2. On the other hand, in the second cationic complex of [PtCl₂(2,2'-bipy)₂]²⁺, the platinum (IV) ion chelated to two 2,2'-bipy ligands through four nitrogen atoms creating a five-member ring and two chloride ions in cis geometry, Fig. 1b. Moreover, a distorted octahedral can be utilized to describe the coordination geometry around the Pt1. With dihedral angles of 79.66°, the 2,2'-bipy ligands are almost perpendicular to one another plane. The length of Pt1–Cl1 is 2.302(13) Å, similar to other platinum chloride complexes [35, 36]. On the other hand, Pt1–N distances range from 2.027(4) Å to 2.044(4) Å, which are similar to those reported in Pt complexes related to those containing a 2,2'-bipyridyl fragment [37, 38]. Table 2 shows the range of cis ∠N–Pt–N bond angles: 80.54(16)° to 96.56(15)°.

In the crystal structure of **SC 1**, the anionic complex of [Pt(Cl)₆]²⁻ is linked to the cationic complex; [PtCl₂(2,2'-bipy)₂]²⁺ through H-bonds forming linear 1D chains. The chloride ions in the anionic complex; [Pt(Cl)₆]²⁻ and hydrogen atoms of the 2,2'-bipy ligand in the cation complex of [PtCl₂(2,2'-bipy)₂]²⁺ participate in intermolecular hydrogen bonds, C6–H6⋯Cl4 = 2.740 Å, C7–H7⋯Cl4 = 2.897 Å, C3–H3⋯Cl3 = 2.883 Å, Fig. S1, Table 3. Furthermore, the 1D chain is extended to the 2D layer via hydrogen bonds formed between the hydrogen atoms of 2,2'-bipy ligands in one chain and the chloride ion in another adjacent chain, C3–H3⋯Cl4 = 2.885 Å, C4–H4⋯Cl2 = 2.779 Å, Fig. 2, Table 3. Thus, the structure is extended into a three-dimensional network by the strong, widespread hydrogen bonding, Fig.S2. Within one edge of the six-membered rings of the 2,2'-bipy ligands exhibit staggered (parallel displaced) intermolecular π-π stacking interactions in the supramolecular complex **1**; (C7–C8 = 3.672 Å, C7–C9 = 3.760 Å, C3–C4 = 3.942 Å), Fig. 3a. So, the 3D supramolecular network structure of **1** that connects the cation and anionic complexes is stabilized by the π-π stacking interactions with centroid–centroid distance 4.125 Å, and intermolecular hydrogen bonds, Fig. 3a, b.

In comparison, the **SC 1** with previously reported [PtCl₂(C₁₀H₈N₂)₂] Cl₂·H₂O, (**2**), the mononuclear complex **2** was synthesized by slow evaporation from a CH₂Cl₂ solution [39]. Pt⁴⁺ ion is six-coordinated in a distorted octahedral environment by four N atoms from the two 2,2'-bipyridine ligands and two chloride atoms as in the cationic complex [PtCl₂(2,2'-bipy)₂]²⁺ in complex (**2**). However, in our binuclear **SC 1** there is another anionic complex (counter ion) of [Pt(Cl)₆]²⁻ with distorted

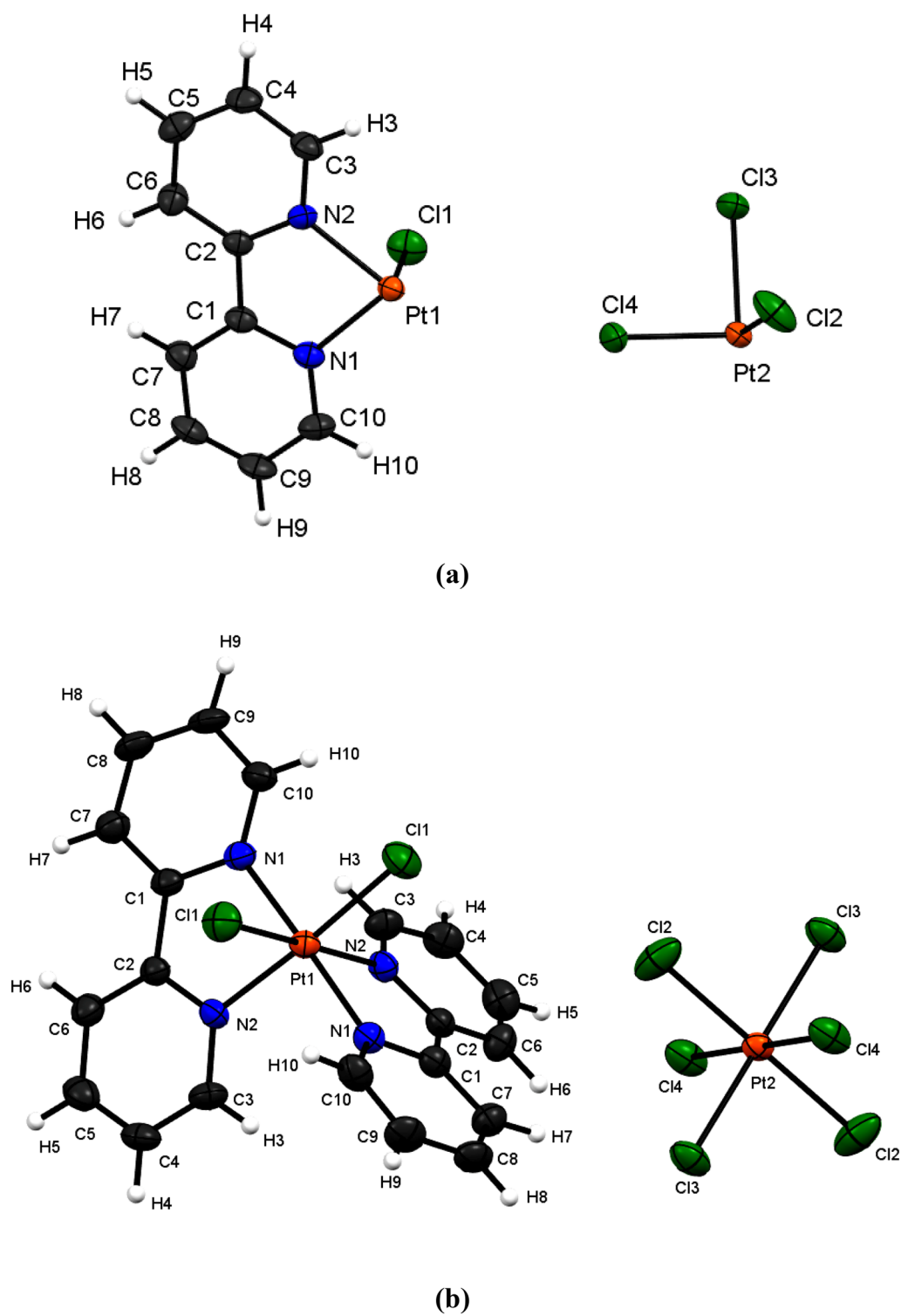


Fig. 1 a Asymmetric unit of **SC 1**, b ORTEP plot of **SC 1** showing the coordination environment around the platinum ion with ellipsoids drawn at 50% probability level

Table 3 Donor–acceptor distances, hydrogen bond lengths, and angles in **SC 1**

D-A...H	d(D-H)/Å	d(H-A)/Å	d(D-A)/Å	D-H-A/°
C3–H3...Cl3 ^a	0.95	2.88	3.640(5)	137.4
C3–H3...Cl4 ^b	0.95	2.85	3.507(5)	126.8
C4–H4...Cl2 ^a	0.95	2.78	3.694(6)	162.1
C6–H6...Cl4 ^c	0.95	2.74	3.364(5)	124.0
C7–H7...Cl4 ^c	0.95	2.90	3.664(6)	138.6
C9–H9...Cl4 ^d	0.95	2.70	3.644(6)	172.4
C10–H10...Cl1	0.95	2.72	3.314(6)	121.2
C3–H3...N1	0.95	2.64	3.174(6)	116.2

^a 1/2-X, -1/2 + Y, 1/2-Z^b + X, 1-Y, -1/2 + Z^c 1-X, +Y, 1/2-Z^d 1/2-X, 1/2 + Y, 1/2-Z

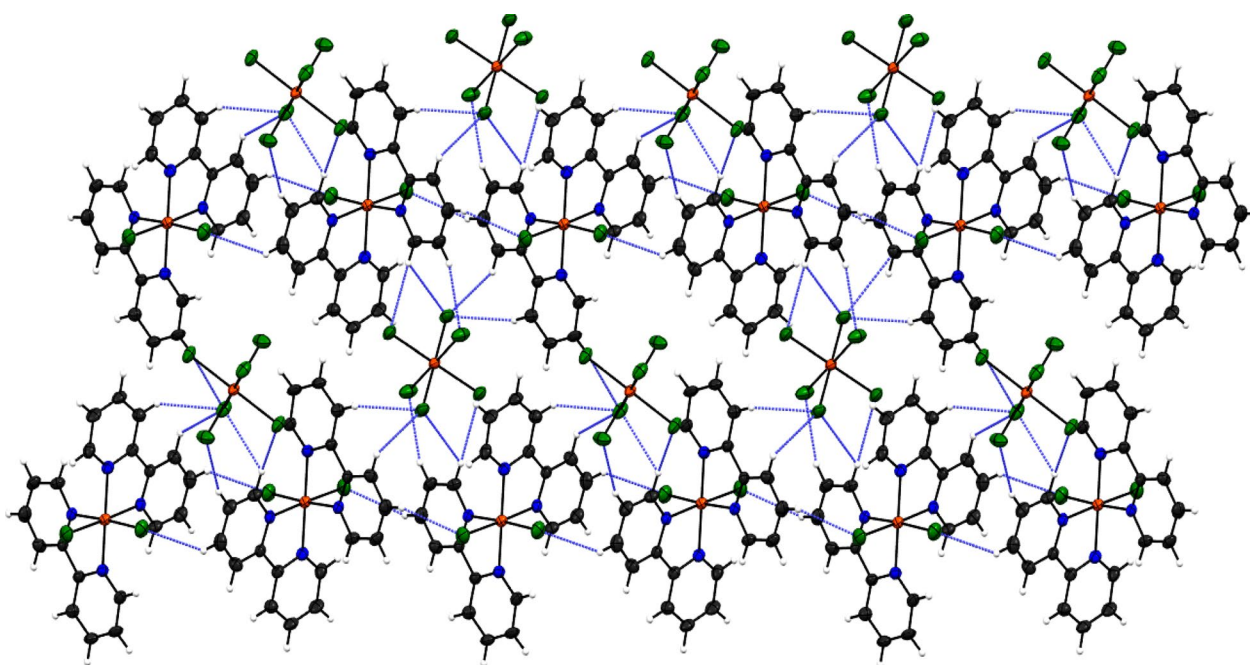
octahedral geometry around the second Pt⁴⁺ ion. The cationic complex [PtCl₂(2,2'-bipy)₂]²⁺ is connected to the anionic complex [Pt(Cl)₆]²⁻ in the crystal structure of **SC 1** via H-bonds. Furthermore, In complex (**2**) there are two chloride ions as counter ions and one water of crystallization responsible for intermolecular hydrogen bonding. The crystal structure confirms a distorted octahedral geometry around the Pt(IV) centers. Extensive hydrogen bonding and π–π stacking interactions lead to a robust three-dimensional network.

IR spectra

Infrared spectra of free ligand 2,2'-bipy and **SC 1** were recorded as KBr belt in 4000–400 cm⁻¹ range, Table 4 and Fig.S3. The infrared spectrum of **SC 1** displays the characteristic bands due to 2,2'-bipy ligand vibrations. In the infrared spectrum of **SC 1**, the stretching mode of the aryl C-H bond is observed at 3088 and 3072 cm⁻¹. Meanwhile, the bands at 1454 and 761 cm⁻¹ are labeled to δ_{CH} and γ_{CH} of 2,2'-bipy ligand. The ν_{CH}, δ_{CH} and γ_{CH} bands were moved to a wavenumber that was greater than the frequency of vibration of 2,2'-bipy free ligand (3069, 3054 1421 and 755 cm⁻¹) supporting hydrogen bond formation [40], Table 4. The ν_{C=N} and ν_{C=C} stretching modes of the 2,2'-bipy ring are present at 1601, 1568 and 1500 cm⁻¹ in the spectrum of **SC 1**, Table 4. Furthermore, the skeletal and C–C vibrations appear at 1311, 1249, 1183 and 1071 cm⁻¹ in the spectrum of **SC 1**, Table 4. In support of the coordination of 2,2'-bipy to the Pt(IV) ion, the ν_{C=N}, ν_{C=C}, and C–C vibrational bands occur at distinct wave numbers, either higher or lower than those of the 2,2'-bipy ligand.

NMR spectra

The distinctive peaks of the 2,2'-bipy ligand are visible in the NMR spectra of **SC 1**. Four multiplet peaks, centered at 8.17, 8.61, 8.95, and 9.35 ppm in the ¹H-NMR spectrum of **SC 1**, are observed, which correspond to the four aromatic protons of the 2,2'-bipy ligand (Fig.

**Fig. 2** Two-dimensional hydrogen bond interactions between the cationic and anionic units that extend the structure into a layered network in **SC 1** along the b-axis

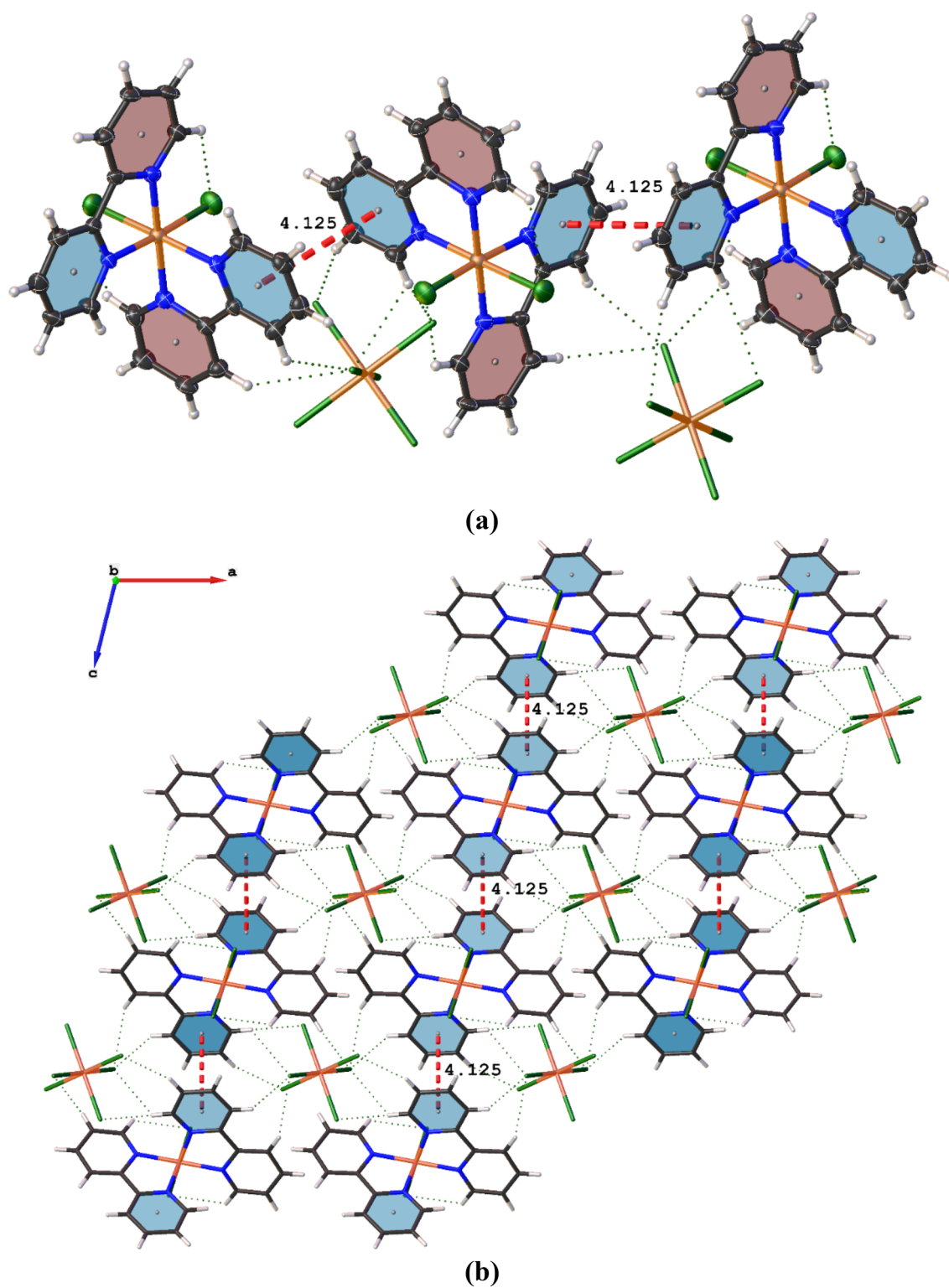


Fig. 3 **a** Three-dimensional network structure of **SC 1** showing pronounced π - π stacking interactions between adjacent 2,2'-bipyridine ligands; **b** extended network stabilized by additional intermolecular hydrogen bonds along the *c*-axis

Table 4 A comparison of vibrational modes before and after coordination provides evidence for the successful formation of SC 1

Compound	ν_{CH} (arom)	$\nu_{\text{C=N}}$ $\nu_{\text{C=C}}$	Skeletal and C–C vibrs. of L	δ_{CH} of L	γ_{CH} of L
2,2'-bipy	306 9w	1684 s	1266 s–1211 w	1421 s	755 m
	3054 w	1552 s	1147 m–1090 s		
SC 1	3088 w	1601 s	1311 s–1249 s	1454 s	761 s
	3072 w	1568 w	1183 m–1071 s		
		1500 s			

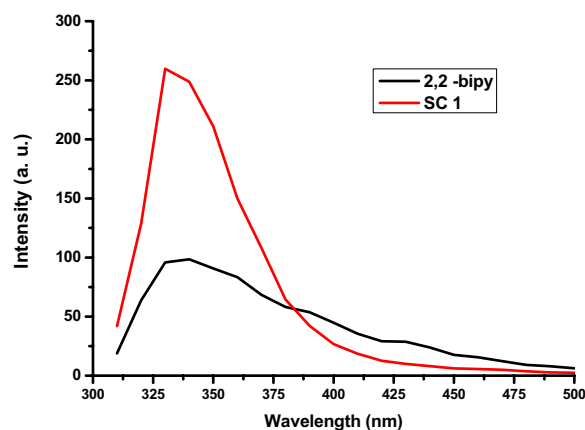
s strong, m medium, w weak

S4). The $^1\text{H-NMR}$ spectrum of free 2,2'-bipy was consulted to support this assignment. It shows strong peaks at 7.12, 7.65, 8.49, and 8.58 ppm, which correspond to the 2,2'-bipy molecules H(4,4'), H(5,5'), H(3,3') and H(6,6'). Almost all of the signals in the $^1\text{H-NMR}$ spectrum of the SC 1 exhibit a discernible downfield shift compared to the spectrum of the free 2,2'-bipy ligand. The shift in peaks is due to the chelation of 2,2'-bipy ligand to the Pt(IV) ion. In the $^1\text{H-NMR}$ spectrum of SC 1, the signal at 3.53 ppm is attributed to the presence of water in the solvent. At 2.5 ppm, the DMSO protons exhibit a prominent singlet band.

All carbon resonances in the $^{13}\text{C-NMR}$ spectra of SC 1 show a considerable downfield shift when compared to the free 2,2'-bipy ligand's spectrum (121.4, 123.6, 137.2, 149.2, and 155.3 ppm). This shift is caused by an electron-density transfer from the ligand to the platinum atoms. Because there are five distinct carbon atoms in the 2,2'-bipy ring, the $^{13}\text{C-NMR}$ spectrum of SC 1 shows five singlet peaks at 127.46, 131.0, 144.84, 148.40, and 155.15 ppm, Fig.S5. As a result, SC 1's NMR spectrum coincide with its structure, which is further supported by X-ray investigation.

The UV-vis and emission spectra

The UV-vis spectra of the free ligand of 2,2'-bipy and SC 1 were investigated in DMF with a concentration 1×10^{-5} M. The UV-vis spectrum of 2,2'-bipy shows two broad bands at 215 and 270 nm associated with $^1\text{L}_a \leftarrow ^1\text{A}$ and $^1\text{L}_b \leftarrow ^1\text{A}$ transition [41]. Furthermore,

**Fig. 4** Emission spectra of the free 2,2'-bipyridine ligand and SC 1 measured in DMF at ambient temperature with an excitation wavelength of 290 nm

a band corresponding to $n-\pi^*$ transitions is visible in the UV-vis spectrum of free ligand 2,2'-bipy at 315 nm. This band disappeared in the UV-vis spectrum of SC 1 as due to ligand's coordination with the Pt(IV) ion [41], Fig. S6, Table 5. Moreover, the electronic absorption spectrum of SC 1 in DMF exhibits only an absorption broad band centered at 285 nm corresponding to $^1\text{L}_b \leftarrow ^1\text{A}$ [41], Fig. S6, Table 5.

The emission spectra of 2,2'-bipy ligand and SC 1 were measured in DMF at ambient temperature, and an excitation wavelength of 290 nm, Table 5 and Fig. 4. A well-developed broad peak is apparent in the emission spectra of 2,2'-bipy and SC 1 at 330–340 nm and 330–337 nm, which correspond to the close-lying $\pi-\pi^*$ transition. In contrast, the 2,2'-bipy ligand's intra-ligand emission $\pi-\pi^*$ is responsible for the weak peak in the emission spectrum at 360 nm [42], Fig. 4, Table 5. Furthermore, the metal-to-ligand charge transfer (MLCT) is responsible for the final peak in the emission spectrum of SC 1 at 350 nm [43]. The fluorescence intensity of SC 1 is higher than that of the free ligand 2,2'-bipy due to its stronger rigidity and ligand coordination [44]. An alternative explanation for the increased fluorescence intensity could be the coordination of the Pt(IV)

Table 5 Electronic absorption and emission spectral data for 2,2'-bipyridine and assignments of electronic transitions of SC 1

λ_{abs} (nm)			λ_{em} (nm)		
2,2'-bipy	SC 1	Assignment	2,2'-bipy	SC 1	Assignment
215		$^1\text{L}_a \leftarrow ^1\text{A}$	330–340 ^b	330–337 ^b	Close lying $\pi-\pi^*$ transition
270	285 ^b	$^1\text{L}_b \leftarrow ^1\text{A}$	360		Intra-ligand emission $\pi-\pi^*$
315		$n-\pi^*$		350	MLCT

^b Broad

ion with the free ligand 2,2'-bipy, which would lessen the intra-ligand excited state's non-radiative decay.

The FT-IR and NMR data confirm successful coordination of the ligand to the platinum centers. The UV–vis and emission spectra reveal important electronic transitions, including the MLCT, which supports the complex's structural integrity.

Studies of DNA binding

DNA binding study by electronic absorption

For examining the properties of compounds that bind to DNA, the electronic absorption titration method is considered to be among the most efficient methods available. In this study, absorption spectral titrations were performed with **SC 1**, maintaining a constant concentration for each titration while incrementally adding CT-DNA in Tris–HCl buffer solution (pH 7.4). Following each addition of CT-DNA, the mixtures were incubated for 5 min at room temperature before taking measurements. The resulting spectra, shown in Fig. 5a, displayed a gradual increase in peak intensity in the 350–400 nm region (hyperchromism) along with a slight shift to a lower wavelength (hypsochromic shift).

A hyperchromic effect, characterized by an increase in absorbance, along with a hypsochromic shift, indicative of a lower wavelength shift, suggests groove binding. The hyperchromic effect occurs because the binding of a molecule to the DNA grooves can cause unwinding or disruption of base stacking interactions, exposing the DNA bases to the solvent and enhancing absorbance.

The hypsochromic shift signifies changes in the electronic environment of the DNA bases, expanding the difference in energy between the excited and ground states. Groove binding induces these changes by causing conformational alterations in the DNA helix without fully intercalating between base pairs. Groove binders fit into the major or minor grooves of the DNA helix, interacting with the edges of the base pairs and causing minor distortions in the DNA structure. These interactions disrupt hydrogen bonds and base stacking slightly but do not completely intercalate between the bases, leading to both hyperchromic and hypsochromic effects observed in spectroscopic studies [26, 27].

By using the Wolfe Shimmer equation [45], the ratio of the slope to the intercept value of the plot shown in Fig. 5b yields the binding constant (K_b), which quantifies the binding affinity of **SC1** with CT DNA [45]. The calculated K_b values for the complex is 5.00×10^6 , indicating that **SC 1** has a high binding affinity for CT DNA [46, 47].

DNA viscosity measurements

DNA is subjected to viscosity measurements by adjusting the added **SC 1** concentrations [48]. We can see the following changes in the relative viscosity of DNA in the presence of metal complexes as a result of different complexes interacting with DNA:

- Electrostatic interaction = No effect on relative viscosity.

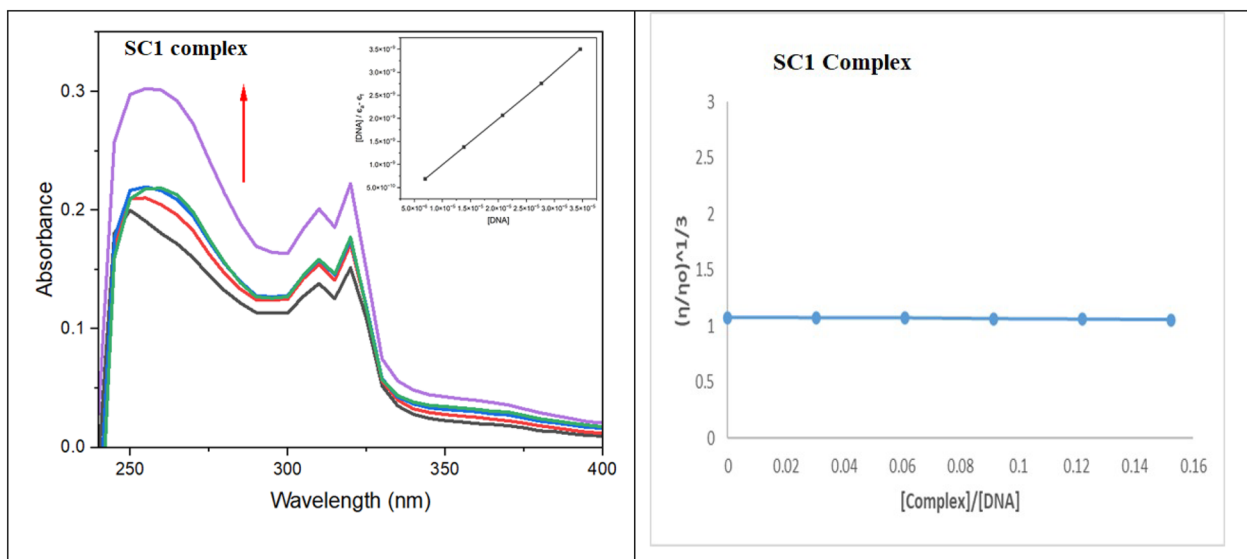


Fig. 5 (Left) Electronic absorption spectra of **SC 1** in Tris–HCl buffer (pH 7.40) upon incremental addition of CT-DNA, showing hyperchromism and a slight hypsochromic shift indicative of groove binding; (Right) Plot of the relative viscosity $[(\eta/\eta_0)^{1/3}]$ versus the $[\text{SC 1}]/[\text{DNA}]$ ratio, confirming the binding mode through minimal viscosity changes

- Intercalative binding = an increase in viscosity.
- Groove binding of DNA = no alteration of the viscosity.
- Covalent interaction = a decreases the relative viscosity.

According to our result, there is any change in viscosity of the DNA with SC 1, which suggests Groove binding with DNA. Electronic absorption titration and viscosity measurements indicate groove binding. Molecular docking results (with DNA and proteins) correlate

well with the experimental data, demonstrating strong interactions.

Molecular docking of SC 1 and different proteins

Docking interactions of SC 1 with 1BNA for DNA sequence

A potent technique for modeling the interactions between small molecules and biomacromolecules is molecular docking. This technique has been used to validate experimental findings further. The two- and three-dimensional models included in the docking results displayed docking scores with extremely low values (Fig. 6). Table 6 presents these findings, which are based

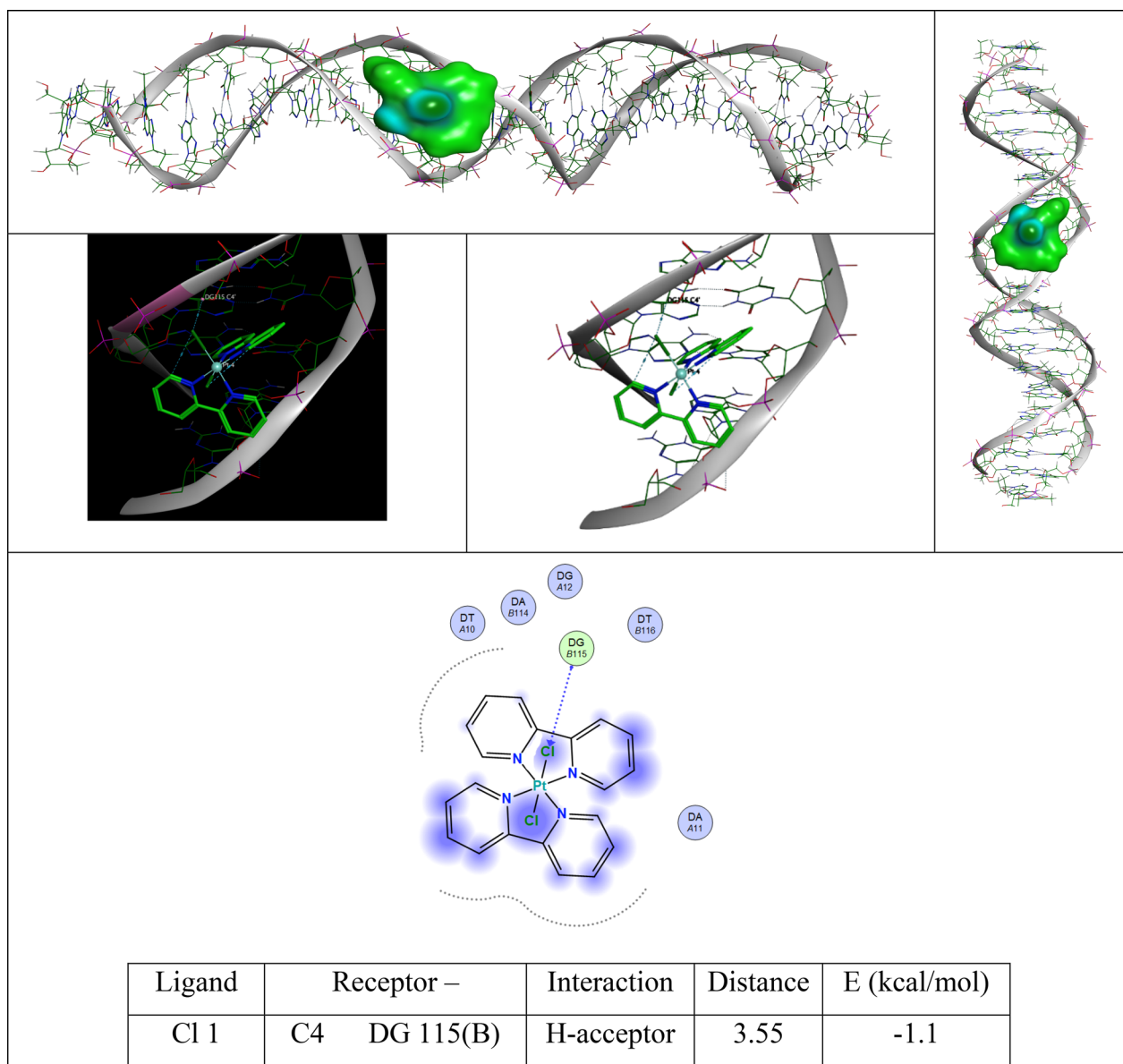


Fig. 6 2D and 3D of the interaction of SC 1 complex with DNA

Table 6 Molecular docking interactions, docking scores, RMSD values and Energetic Parameters of **SC 1** with the DNA Sequence (PDB ID: 1BNA)

mol	S	rmsd_refine	E_conf	E_place	E_score1	E_refine	E_score2
SC 1	-5.37	1.97	-99.70	-10.60	-9.48	-26.49	-5.37
	-5.07	2.08	-99.45	-10.80	-10.32	-24.32	-5.07
	-4.93	2.33	-98.36	-11.67	-12.68	-22.14	-4.93
	-4.84	2.41	-97.78	-11.35	-11.08	-20.36	-4.84
	-4.73	1.98	-97.60	-10.24	-10.56	-20.40	-4.73

on the binding free energy, intermolecular energy, and electrostatic energy that rank highest. The **SC 1** binds within the major groove of DNA, with the chlorine atom forming hydrogen bonds with guanine. Compared to other complexes, **SC 1** has a greater negative binding energy ($S = -5.37$ kcal mol⁻¹), indicating stronger binding to DNA. This finding is consistent with experimental results obtained from electronic absorption spectroscopy and viscosity studies.

Molecular docking of **SC 1** with three different cancer proteins

The **SC 1** was used in molecular docking experiments, Fig. 7 and Table 7 present the docking score (S), (RMSD), and (E) obtained from the analysis. The docking score results indicate that a more -ve docking score signifies improved interaction between the compounds and the different cancer proteins. Additionally, lower RMSD values suggest a more stable docking complex. The energy values correspond to the energy needed for the bioactive compounds to bind to the cancer proteins; therefore, lower energy requirements indicate easier interactions. The redocking results demonstrated that the ligands bound to their targets near their actual conformations, approving the reliability of the docking method and parameters. The docking scores of **SC 1** with the three different cancer proteins, Colon, Breast, and Liver were -7.04, -6.96, and -6.48, reflecting strong binding affinity and consistency with experimental data.

Anticancer evaluation of **SC 1** on human cancer cell lines

HepG2, HCT116, and MDA-MB-231 human cancer cell lines from liver, colon, and breast, were treated for 48 h with varying concentrations (6.25–200 µg/mL) of **SC 1** to assess cell viability in response to the different concentrations of **SC 1**. IC₅₀ values (the concentration at which 50% inhibition occurs) were determined for each cell line. The IC₅₀ for HepG2, HCT116, and MDA-MB-231 were 41.37, 47.62, and 73.90 µM, Table 8. The IC₅₀ values for HepG2 and HCT116 were similar, while MDA-MB-231 IC₅₀ was 1.8 times higher, indicating **SC 1** is more effective against liver and colon cancer cells than against late-stage breast cancer cells.

In addition, the normal human lung fibroblast cell line MRC5 was treated in the same manner as the cancer cell lines to assess **SC 1** cytotoxicity and to calculate the selective index (SI). The SI was obtained by dividing the IC₅₀ of MRC5 by the IC₅₀ of the cancer cell line (Table 8 & Fig. 8). An SI greater than 2 indicates selective cytotoxicity in cancer cells but not in normal cells, Table 8.

Cisplatin was used as a positive control. The results demonstrated that HCT116 and MDA-MB-231 had lower IC₅₀ values than HepG2. The IC₅₀ for HepG2 treated with **SC 1** was like that of cisplatin, while the IC₅₀ values for HCT116 and MDA-MB-231 were 3.6 and 5.2 times higher when treated with **SC 1** compared to cisplatin. The SI values for HepG2 (8.6) and HCT116 (7.2) were higher than for MDA-MB-231 (3.4), indicating **SC 1** is less toxic and more effective as an anticancer agent in HepG2 and HCT116 compared to MDA-MB-231.

Morphological changes and cell growth inhibition were observed in the three cancer cell lines (HepG2, HCT116, and MDA-MB-231) after treatment with 50.7 µM of **SC 1** and 41.6 µM of cisplatin (Fig. 9). Cells treated with **SC 1** and cisplatin exhibited morphological alterations such as spindle or spherical shape changes, abnormal morphology, cytoplasmic constriction, and cell shrinkage.

By comparison, HepG2 and MCF-7 cells have shown anticancer activity against the earlier Pt(IV) supramolecular complex, [Pt(N₃)₆Na₂(phen)₆], with IC₅₀ values of 12.52 ± 1.3 µM for MCF-7 and 23.37 ± 2.1 µM for HepG2 [7]. This complex shows lower cytotoxicity towards normal human lung fibroblast cells [7]. Additionally, the anticancer effects of [Pt(salicylaldimine)(Py)Cl] and the bi-metallic [Pt₂(salicylaldimine)(Py)₂Cl₂] are also sensitive to the HepG2 and MCF-7 cell lines, with IC₅₀ values of 5.8 and 6.3 µM for MCF-7 and 6.1 and 5.9 µM for HepG2 [49]. HepG2 and MCF-7 cancer cells exhibited IC₅₀ values of 20.4 µM and 4 µM, for [Pt(DTBTA)(DMSO)Cl]ClCHCl₃ (DTBTA: 2,2'-dithiobis(benzothiazole)) [50]. Furthermore, the IC₅₀ values for the complexes of trans-[PtCl₂(3-acetylpyridine)₂] and trans-[PtCl₂(4-acetylpyridine)₂] were found to be 27.3 ± 3.7 µM and 13.3 ± 1.5 µM for MCF-7 [51].

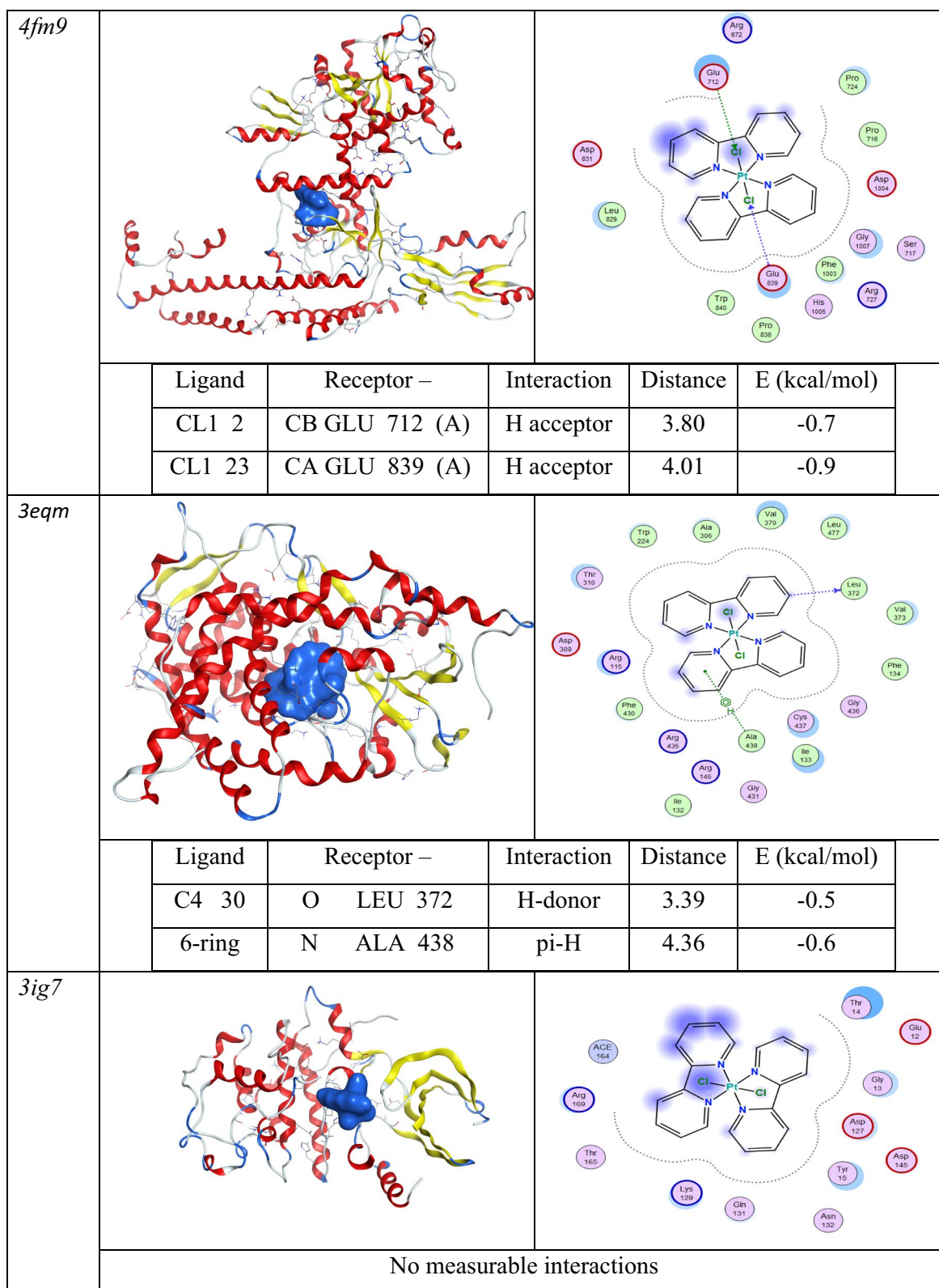


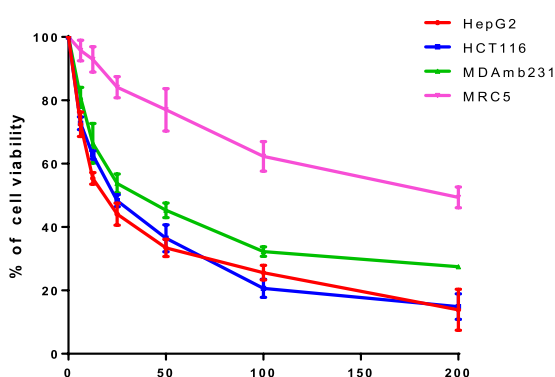
Fig. 7 2D and 3D docking interaction of **SC 1** with cyclin-dependent kinase 5 (*3ig7*), aromatase cytochrome P450 (*3eqm*), and topoisomerase (*4fm9*)

Table 7 Docking scores and energetic parameters of **SC 1** with selected cancer-related proteins (PDB IDs: 3ig7, 3eqm, 4fm9)

mol	S	rmsd_refine	E_conf	E_place	E_score1	E_refine	E_score2
4fm9	-6.48	1.05	-92.58	-70.84	-13.59	-26.81	-6.48
	-6.25	1.61	-98.63	-61.99	-13.85	-22.97	-6.25
	-6.11	1.56	-98.14	-89.69	-14.99	-21.39	-6.11
	-6.09	1.06	-99.19	-76.29	-12.95	-21.50	-6.09
	-5.87	1.54	-98.65	-77.45	-13.15	-18.39	-5.87
3eqm	-6.96	1.06	-78.13	-63.22	-9.80	-29.28	-6.96
	-6.95	2.19	-73.01	-80.96	-9.95	-27.68	-6.95
	-6.93	1.86	-96.29	-89.79	-9.89	-23.12	-6.93
	-6.89	1.31	-97.45	-73.29	-10.26	-24.86	-6.89
	-6.79	1.17	-85.89	-87.08	-10.00	-25.78	-6.79
3ig7	-7.04	1.58	-93.44	-13.29	-11.33	-9.41	-7.04
	-6.92	1.94	-97.08	-41.44	-11.98	-15.65	-6.92
	-6.83	2.29	-97.85	-34.91	-12.14	-18.10	-6.83
	-6.68	2.61	-93.86	-30.83	-11.73	-13.25	-6.68
	-6.51	4.43	-100.30	-21.54	-10.56	-20.62	-6.51

Table 8 Cytotoxicity data, calculated IC₅₀ values, and selectivity indices for **SC1** against HepG2, HCT116, MDA-MB-231, and normal MRC5 cells

SC 1	HepG2	HCT116	MDA	MRC5
Range (µg/mL)	17.25–24.12	20.82–26.48	29.82–44.53	152.5–196.0
IC ₅₀ (µg/mL)	20.40 ± 1.70	23.48 ± 2.5	36.44 ± 0.80	172.9 ± 6.8
IC ₅₀ (µM)	41.37 ± 3.43	47.62 ± 5.7	73.90 ± 1.6	350.66 ± 13.8
SI	8.6	7.2	3.4	
Cisplatin	HepG2	HCT116	MDA	
Range (µg/mL)	8.531–17.07	2.977–5.159	3.282–5.969	
IC ₅₀ (µg/mL)	12.07 ± 1.27	3.919 ± 0.20	4.426 ± 0.88	
IC ₅₀ (µM)	40.23 ± 4.21	13.06 ± 0.66	14.75 ± 2.91	

**Fig. 8** Viability percentage of HepG2, HCT116, MDA-MB-231, and normal cells (MRC5) treated with **SC 1**

Conclusion

This study successfully demonstrates that the design of the novel platinum(IV) supramolecular complex, [PtCl₂(2,2'-bipy)₂](PtCl₆), leads to a unique structural architecture characterized by a distorted octahedral geometry and a robust three-dimensional network formed via hydrogen bonding and π-π stacking. The comprehensive structural characterization, including single-crystal X-ray diffraction and spectroscopic analyses, not only confirms the complex formation but also provides insight into the subtle electronic and geometric modifications imparted by the coordination of the 2,2'-bipyridine ligand. The DNA binding experiments supported by electronic absorption titration and

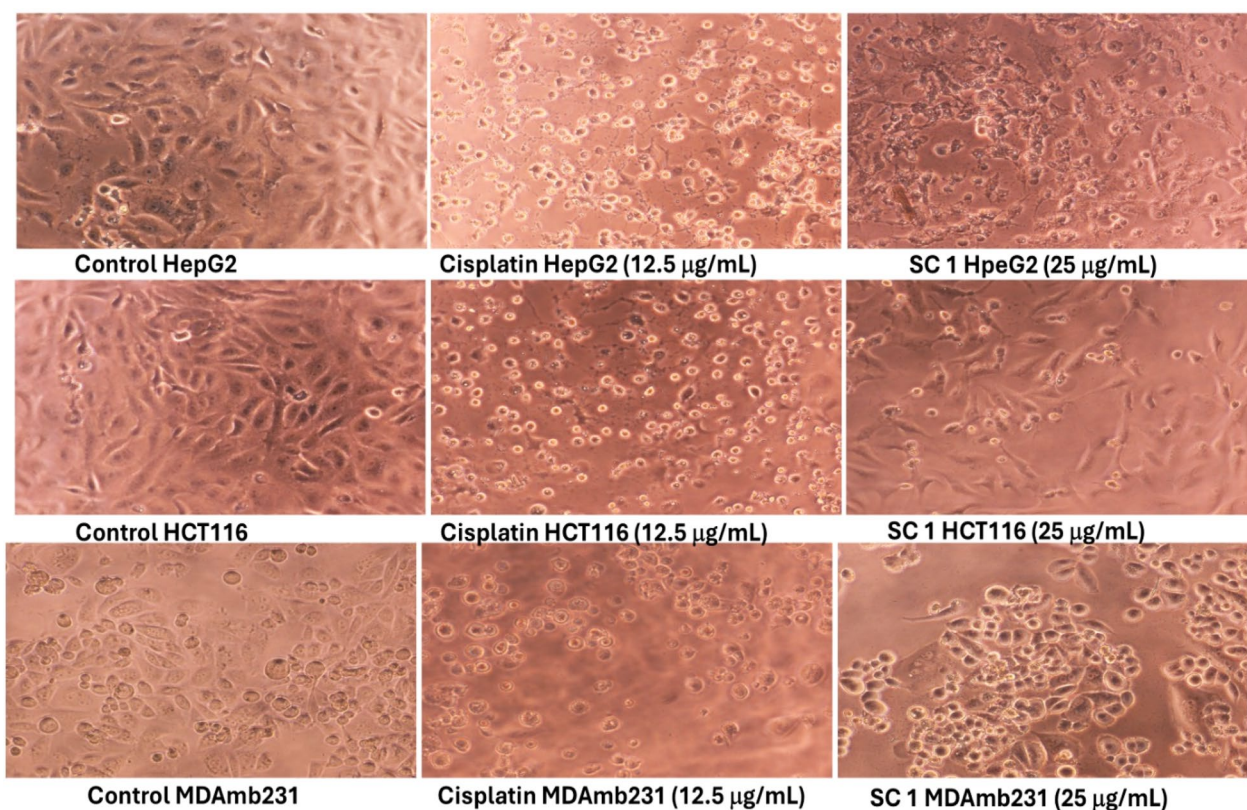


Fig. 9 Images of HepG2, HCT116, and MDAmb231 cells treated with cisplatin (12.5 µg/mL) and **SC 1** (25 µg/mL) after 48 h according to the viability percentage using inverted microscope 20x objective lenses

viscometry indicate that the complex interacts with DNA through groove binding, which is corroborated by molecular docking studies. The strong binding affinity evidenced by the docking scores, along with the observed anticancer activities against HepG2, HCT116, and MDA-MB-231 cell lines, underscores the potential of this complex as a more selective and less toxic alternative to conventional platinum drugs such as cisplatin. Importantly, the study provides a mechanistic framework that correlates the structural features of the complex with its biological activity. This correlation is essential for the rational design of next-generation platinum-based therapeutics that may overcome the limitations of existing treatments. The implications of these findings are significant: not only do they advance our understanding of the structure–activity relationship in platinum-based complexes, but they also pave the way for future studies involving dynamic simulations and *in vivo* evaluations. Future research should focus on optimizing the stability and bioavailability of such complexes and exploring their potential in targeted drug delivery systems. In this regard, our work serves as a promising foundation for the development of safer and more effective anticancer agents.

Supplementary Information

The online version contains supplementary material available at <https://doi.org/10.1186/s13065-025-01472-8>.

Supplementary Material 1

Supplementary Material 2

Acknowledgements

Acknowledgments: This work was funded by the University of Jeddah, Jeddah, Saudi Arabia, under grant No. (UJ-24-DR-3065-1). Therefore, the authors thank the University of Jeddah for its technical and financial support.

Author contributions

Doaa Domyati: conceptualization, project administration, data curation, supervision; Ehab M. M. Ali: methodology, software, writing-original draft preparation, supervision, validation; Mostafa Hussien: writing-original draft preparation, formal analysis, software, data curation; Bambar Davaasuren: investigation, software, formal analysis; Mariusz Jaremko: funding acquisition, methodology, resources, investigation; M. M. El-bendary: conceptualization, methodology, software, writing-original draft preparation, writing-reviewing and editing, data curation, supervision.

Funding

This project was funded by the University of Jeddah, Jeddah, Saudi Arabia, under grant No. (UJ-24-DR-3065-1). Therefore, the authors thank the University of Jeddah for its technical and financial support.

Availability of data and materials

Data will be available upon reasonable request from the corresponding author. Crystallographic data associated with this study has been deposited

at the Chemical Crystallographic Data Centre under the accession number CCDC 2307870. These data can be obtained free of charge via <https://www.ccdc.cam.ac.uk/structures/> or by emailing data_request@ccdc.cam.ac.uk, or by contacting The Cambridge Crystallographic Data Centre, 12 Union Road, Cambridge CB2 1EZ, UK; fax: +44-1223-336033.

Declarations

Ethics approval and consent to participate

Not applicable.

Consent for publication

Not applicable.

Competing interests

The authors declare no competing interests.

Received: 24 February 2025 Accepted: 3 April 2025

Published online: 18 April 2025

References

- Sarto LE, De Gois EP, De Andrade GG, De Almeida MS, Freitas JTJ, Júnior ADSR, Franco LP, Torres C, De Almeida ET, Gouvêa CMCP. Anticancer potential of palladium (II) complexes with Schiff bases derived from 4-aminoacetophenone against melanoma in vitro. *Anticancer Res.* 2019;39:6693–9.
- Carneiro TJ, Martins AS, Marques MPM, Gil AM. Metabolic aspects of palladium (II) potential anti-cancer drugs. *Front Oncol.* 2020;10: 590970.
- Carrera PM, Kantarjian HM, Blinder VS. The financial burden and distress of patients with cancer: understanding and stepping-up action on the financial toxicity of cancer treatment. *CA Cancer J Clin.* 2018;68:153–65.
- Deo KM, Ang DL, McGhie B, Rajamanickam A, Dhiman A, Khoury A, Holland J, Bjelosevic A, Pages B, Gordon C. Platinum coordination compounds with potent anticancer activity. *Coord Chem Rev.* 2018;375:148–63.
- Dominelli B, Correia JD, Kuehn FE. Medicinal applications of gold (I/III)-based complexes bearing N-heterocyclic carbene and phosphine ligands. *J Organomet Chem.* 2018;866:153–64.
- Zou T, Lum CT, Lok C-N, Zhang J-J, Che C-M. Chemical biology of anticancer gold (III) and gold (I) complexes. *Chem Soc Rev.* 2015;44:8786–801.
- El-Bendary MM, Rüffer T, Arshad MN, Asiri AM. Synthesis and structure characterization of Pt (IV) and Cd (II) 1, 10-phenanthroline complexes; fluorescence, antitumor and photocatalytic property. *J Mol Struct.* 2019;1192:230–40.
- El-Bendary MM, Saleh TS, Alomari MM, Ali EM, Davaasuren B, Jaremko M, Babgi BA. Potential anticancer activities and catalytic oxidation efficiency of Platinum (IV) Complex. *Molecules.* 2022;27:4406.
- Etaiw SE-DH, El-Bendary MM. Silver (I) 3-D-supramolecular coordination frameworks constructed by the combination of coordination bonds and supramolecular interactions. *J Coord Chem.* 2010;63:1038–51.
- Etaiw SEDH, El-Bendary MM. Structure and applications of metal-organic framework based on cyanide and 3, 5-dichloropyridine. *Spectrochim Acta Part A Mol Biomol Spectrosc.* 2013;110:304–10.
- Etaiw SEDH, El-bendary MM. Hydrogen bonded 3D-network of silver and 2, 6-pyridinedicarboxylic acid complex: structure and applications. *J Mol Struct.* 2018;1173:7–16.
- Abbass LM, Sadeek SA, Zordok WA, Abdelazi M, El-Attar MS. Mixed ligand 4-hydroxy acetanilide-febuxostat complexes of Co(II), Ni(II), Cu(II) and Zr(IV): Synthesis, structural characterization, DFT calculations, antibacterial, antioxidant and molecular docking studies. *J Mol Struct.* 2024;1308: 138115.
- Wang D, Lippard SJ. Cellular processing of platinum anticancer drugs. *Nat Rev Drug Discovery.* 2005;4:307–20.
- Barnes KR, Kutikov A, Lippard SJ. Synthesis, characterization, and cytotoxicity of a series of estrogen-tethered platinum (IV) complexes. *Chem Biol.* 2004;11:557–64.
- Giandomenico CM, Abrams MJ, Murrer BA, Vollano JF, Rheinheimer MI, Wyer SB, Bossard GE, Higgins JD. Carboxylation of kinetically inert platinum (IV) hydroxy complexes. An entr. acte. ee into orally active platinum (IV) antitumor agents. *Inorg Chem.* 1995;34:1015–21.
- Wang X, Guo Z. Targeting and delivery of platinum-based anticancer drugs. *Chem Soc Rev.* 2013;42:202–24.
- Wexselblatt E, Gibson D. What do we know about the reduction of Pt (IV) pro-drugs. *J Inorg Biochem.* 2012;117:220–9.
- El-Bendary MM, Akhdhar A, Al-Bogami AS, Domyati D, Kalantan AA, Alzahrani FA, Alamoudi SM, Sheikh RA, Ali EM. Palladium and platinum complexes based on pyridine bases induced anticancer effectiveness via apoptosis protein signaling in cancer cells. *Biomaterials.* 2024;37:1–17.
- Abd El-Hamid SM, Sadeek SA, Sadek NB, Sabry MA, El-Gedamy MS. Novel nano-sized metal complexes based on aceclofenac and glycine ligands: synthesis, characterization, molecular docking studies and their enhanced efficacy in ameliorating testicular and spermatological oxidative damages in male rats. *J Mol Liq.* 2023;391: 123274.
- Johnstone TC, Suntharalingam K, Lippard SJ. The next generation of platinum drugs: targeted Pt (II) agents, nanoparticle delivery, and Pt (IV) prodrugs. *Chem Rev.* 2016;116:3436–86.
- Hosseini-Hashemi Z, Moghadam ME, Mirzaei M, Notash B. Biological activity of two anticancer Pt complexes with a cyclohexylglycine ligand against a colon cancer cell line: theoretical and experimental study. *ACS Omega.* 2022;7:39794–811.
- Hosseini-Hashemi Z, Moghadam ME, Notash B, Mirzaei M. Structure-bioactivity relationship study on anticancer Pd and Pt complexes with aliphatic glycine derivative ligands. *Spectrochimica Acta Part A Mol Biomol Spectrosc.* 2024;317: 124408.
- Dolomanov OV, Bourhis LJ, Gildea RJ, Howard JA, Puschmann H. OLEX2: a complete structure solution, refinement and analysis program. *J Appl Crystallogr.* 2009;42:339–41.
- Sheldrick GM. SHELXT-integrated space-group and crystal-structure determination. *Acta Crystallogr Sect A Found Adv.* 2015;71:3–8.
- Sheldrick GM. A short history of SHELX. *Acta Crystallogr A.* 2008;64:112–22.
- Devi CS, Thulasiram B, Satyanarayana S, Nagababu P. Analytical techniques used to detect DNA binding modes of ruthenium (II) complexes with extended phenanthroline ring. *J Fluoresc.* 2017;27:2119–30.
- Alshaikh NE, Zaki M, Sharfalddin AA, Al-Radadi NS, Hussien MA, Hassan WM. Synthesis, structural characterization, DNA/HSA binding, molecular docking and anticancer studies of some D-Luciferin complexes. *Arab J Chem.* 2023;16: 104845.
- Villareal W, Colina-Vegas L, Visbal G, Corona O, Correa RS, Ellena J, Cominetti MR, Batista AA, Navarro M. Copper (I)-phosphine polypyridyl complexes: synthesis, characterization, DNA/HSA binding study, and antiproliferative activity. *Inorg Chem.* 2017;56:3781–93.
- Pozo K, Bibb JA. The emerging role of Cdk5 in cancer. *Trends Cancer.* 2016;2:606–18.
- Sharfalddin AA, Emwas AH, Jaremko M, Hussien MA. Transition metal complexes of 6-mercaptopurine: characterization, theoretical calculation, DNA-binding, molecular docking, and anticancer activity. *Appl Organomet Chem.* 2021;35: e6041.
- Eweas AF, Khalifa NM, Ismail NS, Al-Omar MA, Soliman AMM. Synthesis, molecular docking of novel 1, 8-naphthyridine derivatives and their cytotoxic activity against HepG2 cell lines. *Med Chem Res.* 2014;23:76–86.
- Gurung AB, Bhattacharjee A, Ali MA. Exploring the physicochemical profile and the binding patterns of selected novel anticancer Himalayan plant derived active compounds with macromolecular targets. *Inform Med Unlocked.* 2016;5:1–14.
- Ali EM, Elashkar AA, El-Kassas HY, Salim EI. Methotrexate loaded on magnetite iron nanoparticles coated with chitosan: biosynthesis, characterization, and impact on human breast cancer MCF-7 cell line. *Int J Biol Macromol.* 2018;120:1170–80.
- Plumb JA. Cell sensitivity assays: the MTT assay. In: *Cancer cell culture: methods and protocols.* Springer; 2004. p. 165–9.
- Chen J-L, Tan X-Z, Chen X-X, Wang J-Y, Cao X-F, He L-H, Hua J-Y, Wen H-R. Luminescent mononuclear Pt (II) chloride complexes with C-linked 2, 2'-bipyridyl tetrazole terdentate chelating ligands. *Inorg Chem Commun.* 2013;30:120–3.
- Koo C-K, Ho Y-M, Chow C-F, Lam MH-W, Lau T-C, Wong W-Y. Synthesis and spectroscopic studies of cyclometalated Pt (II) complexes containing

- a functionalized cyclometalating ligand, 2-phenyl-6-(1 H-pyrazol-3-yl)-pyridine. *Inorg Chem.* 2007;46:3603–12.
37. Chen Z, Wong KM-C, Kwok EC-H, Zhu N, Zu Y, Yam VW-W. Electrogenerated chemiluminescence of platinum (II) alkynyl terpyridine complex with peroxydisulfate as coreactant. *Inorg Chem.* 2011;50:2125–32.
 38. Wang J, Chen Y, Law YC, Li M, Zhu MX, Lu W, Chui SSY, Zhu N, Che CM. Organo-and hydrogelators based on luminescent monocationic terpyridyl platinum (II) complexes with biphenylacetylide ligands. *Chem Asian J.* 2011;6:3011–9.
 39. Kim N-H, Hwang I-C, Ha K. Bis(2,2'-bipyridine- κ^2 N, N') dichloridoplatinum(IV) dichloride monohydrate. *Acta Crystallogr Sect E.* 2009;E65: m180.
 40. Nakamoto K. Infrared and Raman spectra of inorganic and coordination compounds, part B: applications in coordination, organometallic, and bioinorganic chemistry. John Wiley & Sons; 2009.
 41. Jaffe HH, Orchin M. *Theory and Applications of ultraviolet spectroscopy*, fifth printing. John Wiley and Sons, Inc.; 1970.
 42. Kharat AN, Rahbari ZV. Antituberculosis, antifungal and photoluminescence studies on a Mn (II)–neocuproine complex. *J Chem Res.* 2012;36:34–7.
 43. Yang X, Zhou G, Wong W-Y. Functionalization of phosphorescent emitters and their host materials by main-group elements for phosphorescent organic light-emitting devices. *Chem Soc Rev.* 2015;44:8484–575.
 44. Boghaei DM, Behzadian AF. Synthesis, characterization and fluorescence spectra of mixed ligand Zn (II), Cd (II) and Hg (II) complexes with 1, 10-phenanthroline-5, 6-dione ligand. *J Coord Chem.* 2007;60:1629–35.
 45. Aziz SG, Elroby SA, Jedidi A, Babgi BA, Alshehri NS, Hussien MA. Synthesis, characterization, computational study, DNA binding and molecular docking studies of chromium (III) drug-based complexes. *J Mol Struct.* 2020;1215: 128283.
 46. Liu Y-X, Mo H-W, Lv Z-Y, Shen F, Zhang C-L, Qi Y-Y, Mao Z-W, Le X-Y. DNA binding, crystal structure, molecular docking studies and anticancer activity evaluation of a copper (II) complex. *Transit Met Chem.* 2018;43:259–71.
 47. Alsaedi S, Babgi BA, Abdellattif MH, Arshad MN, Emwas A-HM, Jaremko M, Humphrey MG, Asiri AM, Hussien MA. DNA-Binding and cytotoxicity of copper (I) complexes containing functionalized dipyriddyphenazine ligands. *Pharmaceutics.* 2021;13:764.
 48. Li Y, Yang Z-Y, Wang M-F. Synthesis, characterization, DNA binding properties, fluorescence studies and antioxidant activity of transition metal complexes with hesperetin-2-hydroxy benzoyl hydrazone. *J Fluoresc.* 2010;20:891–905.
 49. Rahman F-U, Ali A, Khan I, Guo R, Chen L, Wang H, Li Z-T, Lin Y, Zhang D-W. Synthesis and characterization of trans-Pt (II)(salicylaldimine)(pyridine/pyridine-4-carbinol) Cl complexes: in vivo inhibition of *E. coli* growth and in vitro anticancer activities. *Polyhedron.* 2015;100:264–70.
 50. Rubino S, Busà R, Attanzio A, Alduina R, Di Stefano V, Girasolo MA, Orecchio S, Tesoriere L. Synthesis, properties, antitumor and antibacterial activity of new Pt (II) and Pd (II) complexes with 2, 2'-dithiobis (benzothiazole) ligand. *Bioorg Med Chem.* 2017;25:2378–86.
 51. Rakić GM, Grgurić-Šipka S, Kaluđerović GN, Gómez-Ruiz S, Bjelogrić SK, Radulović SS, Tešić ŽL. Novel trans-dichloridoplatinum (II) complexes with 3-and 4-acetylpyridine: Synthesis, characterization, DFT calculations and cytotoxicity. *Eur J Med Chem.* 2009;44:1921–5.

Publisher's Note

Springer Nature remains neutral with regard to jurisdictional claims in published maps and institutional affiliations.